DOI: 10.1021/ma9015505

Macromolecules
ARTICLE

Triggering Mesophase Order in Melts of Metastable, Ultrathin Diblock Copolymer Films through Microstretching: Effect of Melt Film Thickness

Susana Moreno-Flores,*,†,§ Rainer Nehring,† Roberto Raiteri,‡ and Wolfgang Meier*,†

†*Department of Chemistry, University of Basel, Klingelbergstrasse 80, CH-4056 Basel, Switzerland, and* ‡*Department of Biophysical and Electronic Engineering, Via Opera pia 11a, University of Genova, I-16145 Genova, Italy.* §*Current address: Biosurfaces unit, CIC BiomaGUNE, Paseo Miramon 182, E-20009 San Sebastian, Spain.*

Received July 16, 2009; Revised Manuscript Received October 13, 2009

ABSTRACT: By means of a sharp atomic force microscopy (AFM) probe, we have induced the formation of lamellar structures with nanoscale size in ultrathin films of melted poly(1,4-butadiene)-*block*-poly(ethylene oxide) (BD_{84}-EO_{110}, $f_{PB} = 0.55$) at temperatures above the melting temperature of the PEO block and below the order−disorder transition temperature of the copolymer ($T_m < T < T_{ODT}$). The morphology of films 30−50 nm thick is mainly featureless except for the presence of a few monolamellar nanopatches. The absence of an overall lamellar structure, the typical mesophase encountered in this kind of copolymers, suggests that the ultrathin films are arrested in the disordered state. However, repetitive loading−unloading cycles exerted with the AFM probe in the structureless regions lead to the formation of multilamellar islands consisting of 2−9 layers 10−12 nm thick at precise locations. The size, shape, and number of layers of these islands can be controlled by tuning the size of probed area, the loading−unloading rate, and the overall film thickness.

Introduction

Amphiphilic block copolymers composed of hydrophobic−hydrophilic blocks have been attracting great interest in basic research, and (bio)technology.[1] The large variety of self-assembled structures and morphological transformations exhibited by these polymers, either in bulk or dispersed in selective solvents, is the result of the interplay between the molecular structure and the interaction of the blocks. Both the mesophase symmetry and the polymer's capacity to respond under selective physical or chemical conditions have been exploited in lithography[1] and as sensors.[2]

Block copolymers composed of a crystallizable (C-) block and an amorphous (A-) block have received considerable attention because they represent a further step in the degree of structural complexity in block copolymer self-assembly.[3] Below the order−disorder temperature (T_{ODT}), they undergo microphase separation into ordered structures with a defined symmetry called mesophases; however, the order may be altered by the crystallization of the C-block, which can template- or breakout-crystallize, preserving or destroying the mesophase, respectively.[3] Extensive studies have been devoted to the influence of C-block crystallization in the mesophase morphology and physical behavior of C−A copolymers ($T_g^A \ll T_m^C < T_{ODT}$).[3] In particular, block copolymers of poly(butadiene)-*block*-poly(ethylene oxide) (the former block in either its hydrogenated or its unsaturated form) have been systematically investigated as bulk model systems for confined crystallization,[4,5] and in blends with poly(butadiene)[6,7] or with other diblock copolymers.[8]

As films, the complexity increases because thickness imposes a further spatial confinement that may alter both crystallization and mesophase ordering. Despite that, the mechanism of C-block recrystallization in thin and ultrathin films has been studied in detail by Reiter et al.,[9,10] whereas other studies rather focused on the influence of C-block crystallization upon the mesophase morphology.[11−15] Nanotechnological applications abound where ultrathin copolymer films are used as lithographic masks, as templates, or as photonic crystals to create a great variety of nanopatterns. This is possible because of the high control over the microdomain morphology and orientation, which is achieved by manipulating the chemistry of the substrate or by applying electrical fields and mechanical perturbations.[16−18] To this effect, atomic force microscopy (AFM) has not only been an invaluable tool for imaging film morphology on the micro- and nanoscale.[19] As nanolithographic tool, the AFM probe has been used to create patterns on polymer films via indentation,[20] local heating,[21] or electrostatic nanolithography.[22]

In this work, we show new insight into the creation of mesophase ordering in ultrathin melt films of a symmetric diblock copolymer of poly(butadiene)-*block*-poly(ethylene oxide) (PB-*b*-PEO) using temperature-dependent AFM as both an imaging and a nanoconstruction tool. Ultrathin melt copolymer films are mainly structureless except for a few monolamellar patches of small size that appear only above a certain thickness threshold. The featureless regions are actually pseudodewetted areas[10] coated with a residual, nanometer thick polymer layer arrested in the disordered state. Through stretching with the microsized AFM tip, piles of a few lamellae can be generated within these regions at desired locations. The mechanically induced formation of the mesophase from the disordered melt depends on the overall film thickness, whereas the size and shape of the mesophase can be controlled by tuning the size of the probed area and the stretching rate. Triggering mesophase order in ultrathin films not only introduces a new kind of nanopatterning, but it can also generate user-defined geometries for investigation of simultaneously occurring template and breakout C-block crystallization in thin films.

Experimental Section

Chemicals. All reagents used for polymer synthesis had the highest purity grade and were used as received, unless otherwise

*Corresponding authors.

 Published on Web 11/11/2009

indicated. 1,3-Butadiene (>99%, Aldrich) and ethylene oxide (>99.8%, Fluka) were stirred at 195 K and distilled from calcium hydride and *n*-Butyllithium before use; in the case of ethlyene oxide, a sodium mirror was additionally used. Tetrahydrofuran (THF) was refluxed in the presence of sodium−potassium alloy, distilled, and stirred to complete dryness before use. Phosphazene base (*t*-BuP$_4$, Fluka, 1.00 ± 0.02 molar in hexane) and *s*-butyllithium (*s*-BuLi, Aldrich, 1.3 molar in hexane) were used as received. Deuterated chloroform ($CDCl_3$, 99.8%, 0.1% DMS, Aldrich) was used to do the ^{1}H NMR measurements.

Synthesis of BD_{84}-EO_{110}. The copolymer was synthesized via anionic polymerization in THF by the use of flame-dried glassware and under water-free conditions.[23] *s*-Buthyllithium was used as the initiator in the presence of *t*-BuP$_4$ (ratio 1.05:1.00) for polymerization of the butadiene block at 193 K. Polymerization was indicated by the appearance of a bright-yellow color in the reaction flask. Capping of the living end of the polybutadiene block was done by the addition of a small amount (4 mL) of ethylene oxide at 203 K, after which the bright-yellow color vanished. The remaining ethylene oxide was then added, and the reaction flask was heated to 313K to start the polymerization of the ethylene oxide block. After 1 day, the reaction product turned a dark-blue color. End-capping of the living end of the ethylene oxide block was performed by the addition of acetic acid, accompanied by a color change in the reaction flask from dark blue to gold. The resulting polymer was precipitated in cold acetone and subsequently dried under vacuum.

Size Exclusion Chromatography. The polydispersity and the number of butadiene monomers (N_n^{BD}) were obtained by high-performance liquid chromatography (HPLC, Agilent 1100 series). Polydispersity = 1.039; N_n^{BD} = 84. The calculated N_n^{BD} from the monomer/initiator ratio was 85.

Nuclear Magnetic Resonance. ^{1}H NMR spectra were recorded in $CDCl_3$ with a Bruker DPX-400 spectrometer (Bruker, Germany) and were used to calculate the number of ethylene oxide monomers (N_n^{EO}) in the PEO block and the ratio of 1,2 to 1,4 butadiene monomers within the PB block (1,2:1,4 ratio). N_n^{EO} = 110; 1,2:1,4 ratio = 0.9/0.1.

Preparation of PB-*b*-PEO Films. Ultrathin copolymer films were prepared by spin-coating (Laurell, WS-400B-6NPP/LITE) on 2 × 2 cm^2 mica substrates. A few drops of polymer solution (1 mg/mL in chloroform) were placed on the substrate and spun at 1000−4000 rpm for 30 s. If not used immediately, the resulting polymer films were kept in argon.

AFM and Nanoconstruction. The experiments were performed in air with a AFM model 5100 (Agilent Technologies) equipped with a 8 × 8 μm^2 piezoelectric scanner and a high-temperature heating stage (from room temperature up to 200 °C). The images of the polymer film topography were obtained using soft intermittent contact so as to avoid dragging forces that may deform the sample, especially at high temperatures. In this mode, the AFM cantilever is set to oscillate close to its resonance frequency so that the cantilever tip repeatedly taps the surface during scanning. Surface topography is registered through counteracting changes in the cantilever vibration amplitude, which is usually kept constant to a value of 80−90% the free amplitude. Silicon AFM cantilevers with nominal spring constant of 0.1 N/m (Mikromasch, Estonia) were used to scan the polymer film topography before and after the nanoconstruction experiments.

The nanoconstruction experiments were performed in air above room temperature (333−353 K) via a systematic, rate-controlled approach and withdrawal of the AFM tip with respect to the sample at defined sample positions. These positions were produced by dividing the sample scan area in a number of small squares and doing loading−unloading cycles at the center of each square. The loading−unloading cycle was performed as follows: the AFM tip was vertically moved toward the sample surface at rates that ranged from 150 to 500 nm/s until a maximum loading force of 15 nN was reached. Then, the AFM tip was withdrawn from the surface at the same speed until complete detachment.

Table 1. Chemical and Physical Properties of the Copolymer PB-*b*-PEO As Obtained from (1) GPC, (2) ^{1}H-NMR, and (3) DSC

M_n (PB)	4560
M_n (PEO)	4830
$n_{BD}^{(1)}$	84
$n_{EO}^{(2)}$	110
1,2/1,4 ratio$^{(2)}$	0.9:0.1
f_{PEO}	0.45
f_{PBD}	0.55
PDI$^{(1)}$	1.083
$T_m^{(3)}$	322 ± 1, 316 ± 2 K

Differential Scanning Calorimetry. The thermal behavior of the copolymer BD_{84}-EO_{110} was studied using differential scanning calorimetry (Perkin-Elmer, DSC 6). The DSC was previously calibrated with 1.7 mg of copolymer, which was introduced in an aluminum capsule and measured against an empty one that was used as reference. Both capsules were subjected to heating−cooling cycles between 273 and 393 K at rates of 5, 10, and 15 K/min. Changes in the heat difference between sample and reference required to keep them at equal temperature throughout the heating−cooling cycle were used to detect thermal transitions.

Characterization of PB-*b*-PEO (BD_{84}-EO_{110}). Table 1 shows the chemical properties of the copolymer synthesized according to the procedure described in the Experimental Section. The copolymer is composed of a block of 84 butadiene monomers and a block of 110 ethylene oxide monomers. The estimated volume fractions of both blocks obtained from their respective densities (d_{PBD} = 0.86 g/cm^3, $d_{PEO}^{amorphous}$ = 1.13 g/cm^3, $d_{PEO}^{crystalline}$ = 1.23 g/cm^3)[24] are close to 0.5. The polydispersity index (PDI) is close to 1 (1.083), as expected from anionic polymerization. The content of 1,4-butadiene in the PB block measured by ^{1}H NMR is 90%. DSC between 293 and 450 K shows that the bulk copolymer undergoes a phase transition within the temperature range 324−333 K. This phase transition occurs at temperatures similar to the melting point of PEO homopolymers and copolymers with 1,4-butadiene,[6] and it is thus attributed to the melting of the PEO block crystals. Because of the fact that the PB block is amorphous, the crystalline nature of the copolymer suggests the existence of regions rich in PEO blocks and hence phase separation.[3]

Results and Discussion

Morphology of PB-*b*-PEO Ultrathin Films at Room Temperature: Film Thickness. Figure 1a shows the microscale topology of films spin-cast at 1000, 2000, and 4000 rpm, which is mainly characterized by dendritic structures that account for 60−70% of the total projected area (Figure 1b). However, the films spin-casted at lower spin rates, that is, 1000 and 2000 rpm, additionally present bilayered patches of variable size and number, although the latter decreases with increasing spin rate. No patches are observed on films obtained at 4000 rpm. The dendritic features outside the patches have a thickness of 7.5 nm (height step 1 in Figure 1c). Dendrite-like structures have been previously observed on ultrathin films of PEO homopolymers and copolymers containing PEO-blocks, and they are typically associated with flat-on lying PEO crystals.[25,26] Dendrite melting occurs when the films are heated to 318 K (Supporting Information), which coincides with the melting temperature of the PEO blocks from calorimetry data. In these regions, the PEO block thus behaves as a homopolymer. The height profile of the patches on top of the dendrites is revealing because it comprises two piled-up layers, which are 6 to 7 and 8 to 8.4 nm thick (height profiles 2 and 3 in Figure 1c). Taking into account that these patches appear

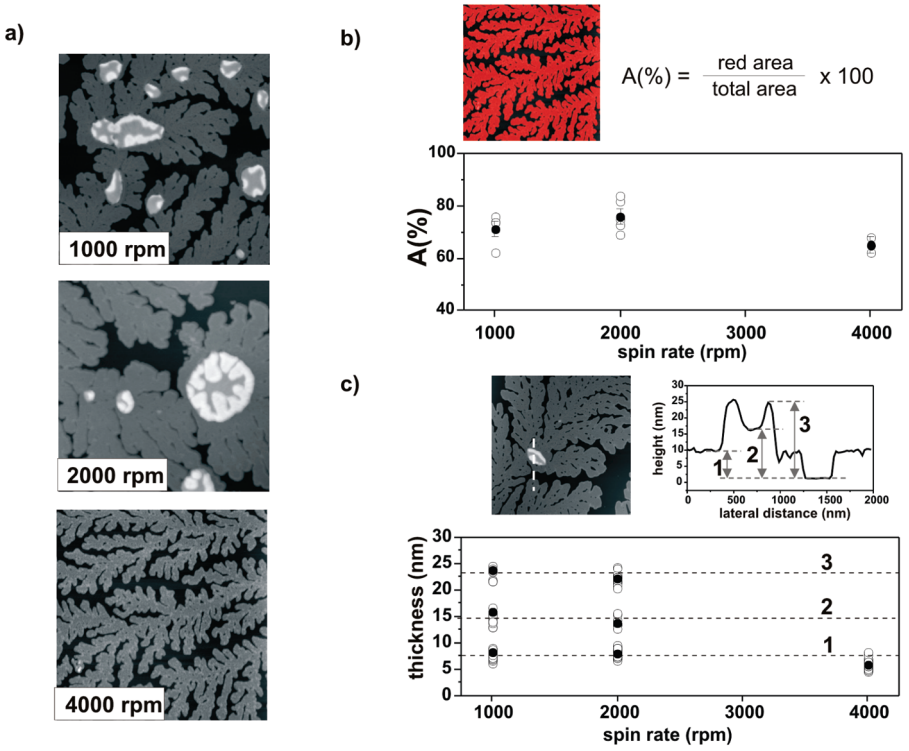

Figure 1. (a) AFM topography images of films of BD_{84}-EO_{110} in intermittent contact mode and in air. Whereas dendritic structures can be seen in all films, lamellar islands are present only on thicker films (i.e., 1000 and 2000 rpm). Height scales from dark gray to white are 27.2, 28.3, and 18.1 nm for the films spin-cast at 1000, 2000, and 4000 rpm, respectively. (b) Calculation of area percentage occupied by dendrites and corresponding plot as a function of spin rate. Filled symbols are average values. Dendrite areas account for 60−70% of the surface showing a slight variation with the spin rate. (c) Height profile along an island and a dendritic structure as indicated in the topography image on the left. Profiles are used to calculate the thickness of each feature relative to the background (dark area). 1000 and 2000 rpm films exhibit three different thickness values corresponding to the dendrite (1) and island heights (2 & 3); on 4000 rpm films, only dendrite thickness can be obtained. Layer thickness are obtained by subtracting the height values 2-1 and 3-2, respectively. Filled symbols correspond again to average values.

only at lower spin rates and that the volume fraction of the PB and the PEO blocks is similar ($f_{PEO} = 0.45$, $f_{PBD} = 0.55$),[24] it is highly probable that they are formed from the excess of polymer material, which spontaneously self-aggregates in the form of parallel, piled-up layers, which is the typical mesophase geometry for this type of copolymers. Layered patches usually appear in thin films of amphiphilic diblock copolymers when the overall amount of material is not commensurate with an integer number of layers.[27] The height of the patches is equal to the lamella thickness in microphase-separated PB-b-PEO,[4] which means that the stacked layers correspond to PB-rich and crystallized PEO-rich mesophases or sublamellae. The top layer appears cracked and discontinuous as a result of the PEO-block crystallization.[4]

As a consequence, these films exhibit two different scenarios for PEO-block crystallization at room temperature: confined in lamellar mesophases and unconfined in disordered, metastable pseudodewetted areas (i.e., breakout crystallization). Moreover, we have found that the lamellar patches do not endure temperatures higher than 423 K (Supporting Information), which is within the range of reported values for the bulk order−disorder transition temperature (T_{ODT}) for poly(butadiene)-*b*-poly(ethylene oxide). The latter varies with the molecular weight of the copolymer, ranging from 405 (4000 g/mol)[8] to >573 K (13 000 g/mol).[28,29] It is thus evident that at room temperature, the patches retain the mesophase order and hence are in thermodynamic equilibrium, whereas this is not the case elsewhere in the film, where it behaves as a "zeroth layer".[30] Outside the patches, the copolymer is thus metastable. Metastability is a required condition for triggering mesophase order at higher temperatures.

Atomic Force Microscopy Probe-Induced Formation of Multilamellar Structures of Nanometer Size (Nanolamellae) in Melt Films. At temperatures above the melting point of PEO crystals, the topology of the films spin-cast at 1000 and 2000 rpm is characterized by large, featureless regions and a few dispersed lamellar patches 12.1 ± 0.1 nm thick. (See images in Figure 2.) Under these conditions, the thickness of the melt film can be obtained by force spectroscopy.[31] Figure 2a shows a typical force versus distance curve obtained at 333 K, in which the deflection force of an AFM cantilever is plotted as a function of the distance of the tip from the polymer film. Upon approaching the substrate, the AFM tip contacts the melted film (point (1) in Figure 2a). The sudden jump-in may be certainly influenced by attractive capillary forces, though. A water layer of 0.5 nm thickness is spontaneously formed on surfaces under ambient air;[32] consequently, a water meniscus is typically formed in the interstitial region between the AFM tip and the sample. However, on further approach, there is almost no change in the deflection force for a few tens of nanometers (region (2) in Figure 2a) before it undergoes a linear increase (point (3) in Figure 2a). Strong capillary forces alone, typically detected as sudden jump-ins of a few nanometers to the subnanometer range and on approach AFM curves,[31] cannot thus account for region (2). A more rational interpretation involves the AFM tip traversing the fluid film at region (2) until it reaches the underlying mica substrate at point (3). At this point, the cantilever deflection force increases because of repulsion with a solid, rigid surface. The length extension between

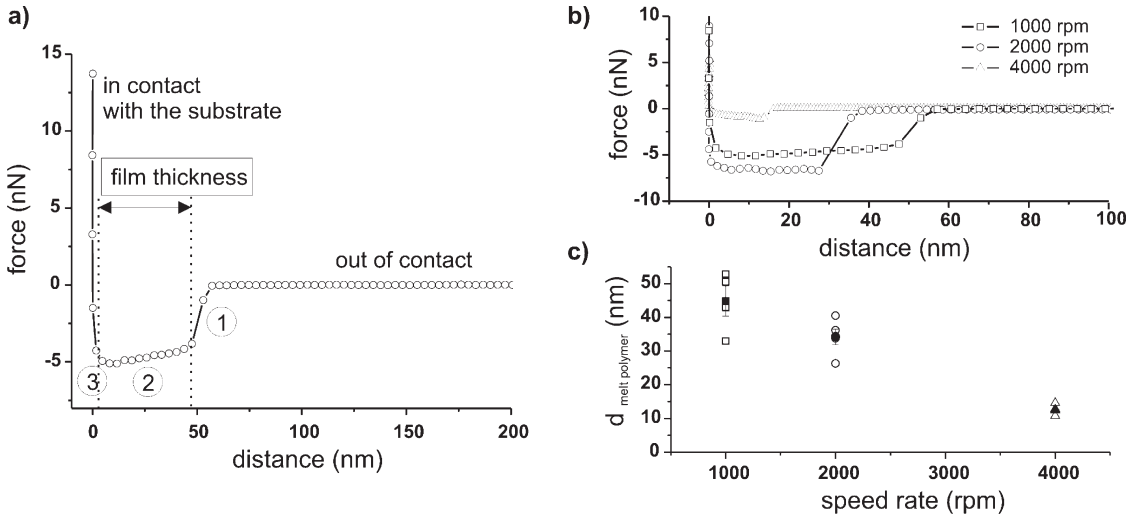

Figure 2. (a) Force versus distance curve on a polymer melt film (1000 rpm) performed in air at 333 K. The curve shows the force probed by the cantilever as a function of the tip-film distance. At large distances, the tip is not in contact with the film. At point (1), the tip touches the film, showing the typical instability at contact. Along the region (2), the tip traverses the film with no notable change in cantilever force until it encounters the solid mica substrate at (3). The extension of the region (2) determines the film thickness. (b) High-temperature force spectroscopy curves performed on polymer melts spin-cast at different spin rates (1000, 2000, and 4000 rpm), where the different extensions of region (2) are noticeable. (c) Film thickness as a function of the spin speed of film formation. As expected, the melt polymer thickness is inversely proportional to the spin speed.

points (1) and (3) thus determines the thickness of the polymer film.

Figure 2b shows force−distance curves on the melted polymer films spin-cast at 1000, 2000, and 4000 rpm. They all exhibit a similar feature, except for the extension of the region (2), which increases in the order 1000 > 2000 > 4000 rpm (Figure 2b). Therefore, the thickness of the melt polymer film decreases with spin rate, as expected for spin-coated films. In particular, a four-fold increase in the spin rate resulted in a 72% decrease in polymer melt film thickness, from 45 nm down to 12.5 nm for 1000 and 4000 rpm films, respectively. Melt polymer thickness is a requirement for nanolamellae construction, as we will show later.

Nanolamellae Construction. We have shown that approach curves in force spectroscopy assist us in determining polymer melt thickness; however, force spectroscopy maps reveal something more. Force curves were systematically performed within a featureless area (generally a rectangular or a square region) of the polymer melt at temperatures above 333 K; the same region is imaged before and after force mapping to check the effect of repetitive film loading−unloading. The result is striking, as Figure 3a shows: where nothing is to be seen before force mapping, a new structure appears thereafter. In this case, Figure 3a shows a three-layer island. These newly created islands generated from the melt are again arranged in layers.

The ability to create these piled structures depends on the amount of polymer melt, which is controlled by sample preparation. The patches are not formed on the thinnest polymer melts, being 12.7 ± 0.8 nm thick, but they appear on thicker melts, with thickness of 45 ± 4 and 34 ± 2 nm, respectively. Force curves performed during tip retraction from the melt (Figure 3b) show a prominent adhesion that extends over long distances away from the substrate. In particular, Figure 3b shows an average unloading curve calculated from hundreds of curves. The depicted distance is the mean adhesion length between tip and surface, $< l_{adh} >$. This quantity can certainly be influenced by capillary forces, which are often responsible for the large adhesion forces encountered at room temperature. However, at medium-high humidity, adhesion forces highly influenced by capillary forces are in the range of 75−300 nN.[33−35] We report a much lower values of 10−15 nN, which are comparable to those encountered at low humidity and even at ultrahigh vacuum,[34] where capillary forces play a minor role. Moreover, water meniscus formation requires that water vapor condenses, which may be highly hindered at the working temperature of our experiments (333 K). However, $< l_{adh} >$ correlates with the island height or, in other words, with the number of layers. The plot in Figure 3c shows that both $< l_{adh} >$ and island height steadily increase with the layer number. Moreover, island height linearly depends on the layer number, which makes it possible to calculate the sublamella thickness from the slope of a linear regression, being 12.5 ± 0.2 nm. This value is slightly higher than that encountered in melt bulk copolymers (10 nm)[4,5,28] and is also higher than the values found in the islands of the as-formed spin-coated films at room temperature (Figure 1). Additionally, the number of induced layers correlates with the overall polymer film thickness; seven-layer and nine-layer islands are formed on 1000 rpm films, two-, three-, and five-layer islands are formed on 2000 rpm films, and zero-layer islands (i.e., no islands) are formed on 4000 rpm films.

The relation found between the mean adhesion length and the number of layers in the so-formed islands suggests that a minimum requirement for island creation is an isotropic melt film thicker than 10 nm and that the underlying mechanism should involve cantilever-induced local microstretching of the polymer film out of molecular scale. Mechanically induced isotropic-to-lamellar transitions in bulk copolymers have been previously reported, where dynamic shearing favored the formation of lamellae in disordered melts of poly(ethylene-propylene)-*b*-(ethylethylene).[36] An alternative explanation for the appearance of the islands may also be random deposition of excess of polymer melt from the AFM tip to the surface as a sort of dip-pen lithographic tool;[37] however, to keep the high degree of order of the planar, pile-arranged islands over large areas makes it seems highly improbable for an erratic material transfer. Moreover, the island projected area was in most cases ~400% larger than the actual probed area (Figure 4a), which invalidates material delivery as the main cause for island formation. Although certain material transfer between the tip and the surface due to successive contacts cannot be avoided,

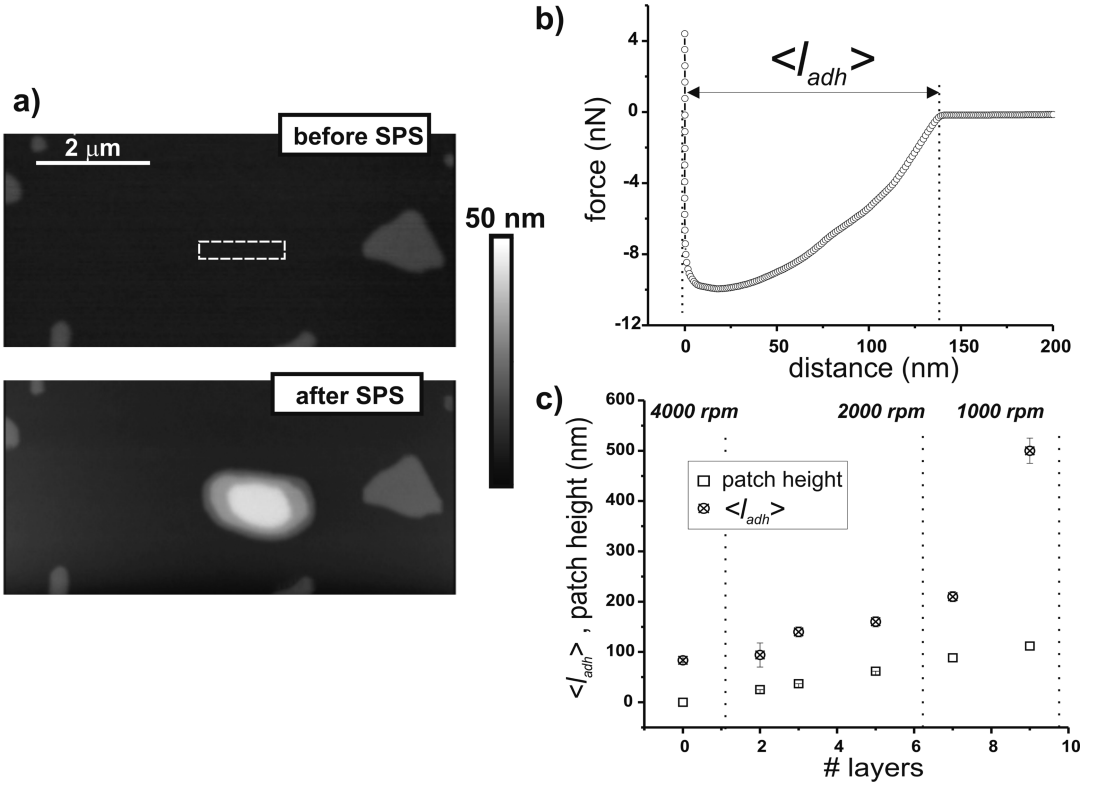

Figure 3. (a) Intermittent contact mode height AFM images of the same region of copolymer melt (2000 rpm, 333 K) before and after a map of 768 force curves taken on a regular grid. The image above shows a wide featureless central area of polymer melt. The rectangle shows the region (1500 × 300 nm^2) where force curves were taken in a regular grid. The image below shows that after force mapping a new three-layer island appears. (b) Average unloading curve within the scanned area. The mean adhesion length, $< l_{adh} >$, is the mean distance required for the tip to completely detach from the melt, calculated from 768 unloading curves. (c) Mean adhesion length and thickness of the created patches as a function of the layer number and the spin rate. Island height is linearly proportional to the lamellae number, which makes it possible to calculate the lamella thickness (12.5 ± 0.2 nm). $< l_{adh} >$ also increases with the lamellae number, and it is significantly higher than the island thickness.

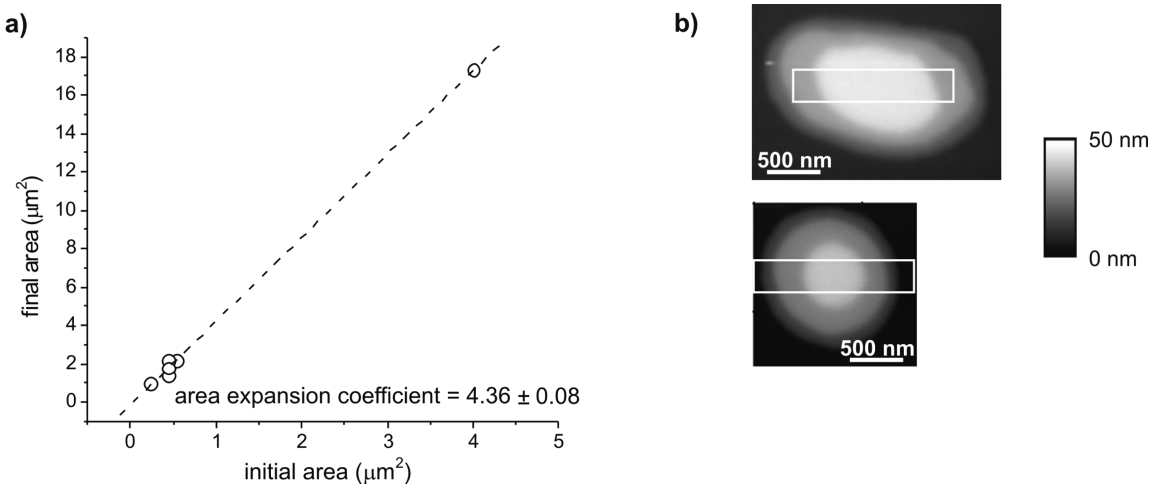

Figure 4. (a) Area expansion coefficient calculated as the ratio between the area of the force curve map and the area of the resulting patch; in all cases, the patch areas are ~400% larger than the theoretical area where no expansion occurs. (For equal areas, the area expansion coefficient would be 1). (b) 3-Lamellae islands formed after taking force curves on a grid over an equivalent area (0.45 μm^2) and at the same maximum loading force (4.7 nN); upper image: loading−unloading rate of 250 nm/s; lower image: loading−unloading rate of 500 nm/s.

mechanical stretching of the melt film thus appears to be the main cause for mesophase formation, which it additionally extends beyond the probed areas, as Figure 4 shows. It is therefore likely that the tip induces molecular arrangements in the neighboring areas, leading to lateral expansion of the lamellae. In this case, microstretching-induced order would be kinetically controlled and hence should depend on loading−unloading rates. Figure 4b shows that scanning equivalent initial areas at loading−unloading rates of 250 and 500 nm/s results in the formation of differently shaped islands with the same number of lamellae. At rates 250 nm/s and below (125 nm/s was also tested), the force curves performed on rectangular areas result in an elliptically shaped three-layered island with its long axis oriented parallel to the long axis of the rectangle. At higher rates (500 nm/s), the formed island has the same number of layers,

but it is round-shaped, and it shows less resemblance to the geometry of the probed area.

Conclusions

Ultrathin melt films of symmetric diblock copolymers PB-*b*-PEO exhibit singular features as a consequence of vertical confinement. Below the order−disorder transition temperature (T_{ODT}), 30−50 nm thick films are metastable and arrested in a disordered state. Mechanical perturbations, that is, stretching, can induce mesophase order in the shape of islands consisting of piled-up layers of half-lamellae thickness at desired locations within the film. The number and the size of the layered islands are restricted because of the small amount of polymer material that is not commensurate with the number of layers and the local nature of the perturbation. Nonetheless, the size, shape, and layer number can be, to a certain extent, controlled by tuning the film thickness, the probed area, and the stretching (i.e., unloading) rate. These observations introduce a new way of controlling melt copolymer film morphology for studying C-block crystallization and ordering processes as well as for nanolithography.

Acknowledgment. S.M.F. and R.N. thank the Marie Curie 6th framework programmes (Nest 043431 and MRTN-CT-2004-005516) for financial support. This work has also been supported by the Swiss National Science Foundation and the NCCR-Nanoscale Science. Kathryn Melzak and Jose Luis Toca-Herrera are kindly acknowledged for manuscript correction and discussions. Kathryn Melzak is additionally acknowledged for providing literature.

Supporting Information Available: Thermal behavior of ultrathin films of symmetric PB-*b*-PEO copolymers. This material is available free of charge via the Internet at http://pubs.acs.org.

References and Notes

(1) *Developments in Block Copolymer Science and Technology*; Hamley, I. W., Ed.; John Wiley & Sons: Chichester, U.K., 2004.
(2) Rusell, T. P. *Science* **2002**, *297*, 964.
(3) Nandan, B.; Hsu, J.-Y.; Chen, H.-L. *J. Macromol. Sci., Part C* **2006**, *46*, 143.
(4) de Jeu, W.-H. In *Lecture Notes in Physics*; Reiter, G., Sommer, J.-U., Eds.; Springer-Verlag: Berlin, 2003
(5) Li, L.; Lambreva, D.; de Jeu, W.-H. *J. Macromol. Sci., Part B* **2004**, *B43*, 59.
(6) Chen, H.-L.; Wu, J.-C.; Lin, T.-L.; Lin, J.-S. *Macromolecules* **2001**, *34*, 6936.
(7) Lee, W.; Chen, H.-L.; Lin, T.-L. *J. Polym. Sci., Part B: Polym. Phys.* **2002**, *40*, 519.
(8) Frielinghaus, H.; Hermsdorf, N.; Almdal, K.; Mortensen, K.; Messé, L.; Corvazier, L.; Fairclough, J.-P.-A.; Ryan, A.-J.; Olmsted, P. D.; Hamley, I.-W. *Europhys. Lett.* **2001**, *53*, 680.
(9) Reiter, G.; Castelein, G.; Hoerner, P.; Riess, G.; Sommer, J.-U.; Floudas, G. *Eur. J. Phys. E* **2000**, *2*, 319.
(10) Reiter, G.; Vidal, L. *Eur. Phys. J. E* **2003**, *12*, 497.
(11) Hong, S.; MacKnight, W. J.; Russell, T. P.; Gido, S. P. *Macromolecules* **2001**, *34*, 2876.
(12) Liang, G.-D.; Xu, J.-T.; Fan, Z.-Q.; Mai, S.-M.; Ryan, A. J. *Polymer* **2007**, *48*, 7201.
(13) Fu, J.; Luan, B.; Pan, C.; Li, B.; Han, Y. *Macromolecules* **2005**, *38*, 5118.
(14) Li, Y.; Loo, Y.-H.; Register, R. A.; Green, P. F. *Macromolecules* **2005**, *38*, 7745.
(15) Opitz, R.; Lambreva, D. M.; de Jeu, W. H. *Macromolecules* **2002**, *35*, 3930.
(16) Park, C.; Yoon, J.; Thomas, E. L. *Polymer* **2003**, *44*, 6725.
(17) Segalman, R.-A. *Mater. Sci. Eng., R* **2005**, *48*, 191.
(18) Chen, J.-Y.; Ross, C. -A.; Smith, H. −I.; Thomas, E. -L. *Adv. Mater.* **2006**, *15*, 2505.
(19) Magonov, S. N. In *Encyclopedia of Analytical Chemistry*; Meyers, R. A., Ed.; John Wiley & Sons: Chichester, U.K., 2000.
(20) (a) Cappella, B.; Bonaccurso, E. *Nanotechnology* **2007**, *18*, 155307. (b) Li, G.-M.; Burggraf, L.-W. *Nanotechnology* **2007**, *18*, 245302.
(21) Vettiger, P.; Brugger, J.; Despont, M.; Drechsler, U.; Duerig, W.; Haeberle, M.; Lutwyche, H.; Rothuizen, H.; Stutz, R.; Widmer, R.; Binnig, G. *Microelectron. Eng.* **1999**, *46*, 101.
(22) Jegadesan, S.; Sindhu, S.; Valiyaveettil, S. *Small* **2006**, *2*, 481.
(23) Nehring, R.; Palivan, C.-G.; Casse, O.; Tanner, P.; Tüxen, J.; Meier, W. *Langmuir* **2009**, *25*, 1122.
(24) Lambreva, D.; Opitz, R.; Reiter, G.; Frederik, P. M.; de Jeu, W.-H. *Polymer* **2005**, *46*, 4868.
(25) Reiter, G.; Sommer, J.-U. *J. Chem. Phys.* **2000**, *112*, 4376.
(26) Huang, Y.; Liu, X.-B.; Zhang, H.-L.; Zhu, D.-S.; Sun, Y.-J.; Yan, S.-K.; Wang, J.; Chen, X.-F.; Wan, X.-H.; Chen, E.-Q.; Zhou, Q.-F. *Polymer* **2006**, *47*, 1217.
(27) Hamley, I. A. *The Physics of Block Copolymers*; Oxford University Press: New York, 1998
(28) Shiomi, T.; Takeshita, H.; Kawaguchi, H.; Nagai, M.; Takenaka, K.; Miya, M. *Macromolecules* **2002**, *35*, 8056.
(29) T_{ODT} as high as 573 K has also been reported, although not measured, for poly(butadiene-*b*-ethylene oxide) in ref 4. Ref 28 states that T_{ODT} should be greater than 573 K because at that temperature, high-order SAXS peaks due to microphase separation are still visible.
(30) (a) Harrison, C.; Park, M.; Chaikin, P. M.; Register, R. A.; Adamson, D. H.; Yao, N. *Polymer* **1998**, *39*, 2733. (b) Harrison, C.; Chaikin, P. M.; Huse, D. A.; Register, R. A.; Adamson, D. H.; Daniel, A.; Huang, E.; Mansky, P.; Russell, T. P.; Hawker, C. J.; Egolf, D. A.; Melnikov, I. V.; Bodenschatz, E. *Macromolecules* **2000**, *33*, 857.
(31) Butt, H.-J.; Cappella, B.; Kappl, M. *Surf. Sci. Rep.* **2005**, *59*, 1.
(32) Beaglehole, D.; Christenson, H.-K. *J. Phys. Chem.* **1992**, *96*, 3395.
(33) Farschdi-Tabrizi, M.; Kappl, M.; Butt, H.-J. *J. Adhes. Sci. Technol.* **2008**, *22*, 181.
(34) Yang, S.-H.; Nosonovsky, M.; Zhang, H.; Chung, K.-H. *Chem. Phys. Lett.* **2008**, *451*, 88.
(35) Wei, Z.; Zhao, Y.-P. *J. Phys. D: Appl. Phys.* **2007**, *40*, 4368.
(36) Koppi, K.-A.; Tirrell, M.; Bates, F.-S. *Phys. Rev. Lett.* **1993**, *70*, 1449.
(37) Piner, R. D.; Zhu, J.; Xu, F.; Hong, S.; Mirkin, C. A. *Science* **1999**, *283*, 661.